Dierk Raabe, Frank Heringhaus[1]), Ude Hangen and Günter Gottstein

(Institut für Metallkunde und Metallphysik, Kopernikusstr. 14, Rheinisch-Westfälische Technische Hochschule Aachen, D-52056 Aachen, Germany)

Investigation of a Cu-20 mass% Nb in situ Composite
Part I: Fabrication, Microstructure and Mechanical Properties

Fiber reinforced in situ metal matrix composites (MMCs) consisting of Cu and 20 mass% Nb were fabricated by large strain cold rolling and wire drawing of a cast ingot. The microstructural evolution of the composites was investigated by means of scanning and transmission electron microscopy. The mechanical properties of the MMCs were discussed on the basis of the microstructural changes during deformation. The results substantiate that the volume density of internal boundaries and the filament spacing have considerable influence on the strength of Cu-20 mass% Nb. The evolution of the strength during deformation was simulated by application of analytical approaches which incorporate experimental data. The results reveal a very good correspondence to the behavior observed. On the basis of the current findings potential industrial applications are discussed.

Untersuchung eines Cu-20 Masse-% Nb in situ-Verbundwerkstoffes
Teil I: Herstellung, Gefüge und mechanische Eigenschaften

Faserverstärkte in situ Metallmatrix-Verbundwerkstoffe (MMCs) bestehend aus Cu und 20 Masse-% Nb wurden durch starke Walz- sowie Drahtverformung aus einem Gussblock hergestellt. Die Mikrostrukturentwicklung des Verbundwerkstoffes wurde mittels Raster- und Transmissionselektronenmikroskopie untersucht. Die Diskussion der mechanischen Eigenschaften der MMCs erfolgte auf der Grundlage der beobachteten Gefügeänderungen. Die Ergebnisse legen nahe, daß die Dichte der inneren Grenzflächen und die Filamentabstände einen beträchtlichen Einfluß auf die Festigkeit haben. Unter Verwendung analytischer Ansätze wurde die Entwicklung der Festigkeit während der Verformung simuliert. Die Ergebnisse weisen eine sehr gute Übereinstimmung mit dem beobachteten Werkstoffverhalten auf. Auf der Basis der gegenwärtigen Resultate werden potentielle industrielle Anwendungen erörtert.

1 Introduction

Cu and Nb have negligible mutual solubility in the solid state [1, 2]. Hence, fiber reinforced in situ processed metal matrix composites (MMCs) can be manufactured by large degrees of deformation, e.g. by wire drawing or cold rolling of a cast ingot. Heavily deformed Cu-Nb MMCs reveal a very high strength and good electrical conductivity. Both the mechanical properties and the electrical conductivity of Cu-Nb considerably exceed those of competitive alloys like Cu-Be, Cu-Ni, Cu-Ni-Mn, Cu-Ta or Cu-Cr (Fig. 1). Decreasing the Nb content leads to a loss of strength and increasing the Nb content leads to the degradation of ductility and electrical conductivity (Fig. 1). Thus, an alloy containing 20 mass% Nb appears to combine optimum electrical and mechanical properties [3 to 8]. Cu-Nb composites have been under intensive investigation in the past [1 to 16] mainly for two reasons:

i. From a scientific point of view Cu-20 mass% Nb is a very challenging material, since its tensile strength after deformation is very high, in particular much greater than expected from the rule of mixtures [3 to 9] (Fig. 2). Several models have been proposed to explain the strength observed. The barrier model by Spitzig et al. [7 to 9, 11] attributes the strength to the difficulty of propagating plastic flow through the fcc-bcc interfaces (fcc = face centered cubic, bcc = body centered cubic). Funkenbusch and Courtney interpret [10] the strength in terms of geometrically necessary dislocations owing to the incompatibility of plastic deformation of the bcc and fcc phase. In fact, both models succeed in describing the observed increase of strength assuming reasonable fitting parameters. In a recent approach, Raabe and Hangen
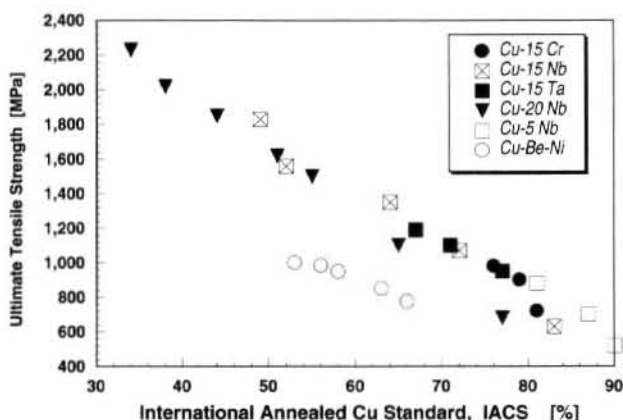

Fig. 1. Ultimate tensile strength versus international annealed Cu standard, IACS, of various Cu based alloys.

[1]) Now with: National High Magnetic Field Laboratory, Tallahassee, Florida 32306, USA
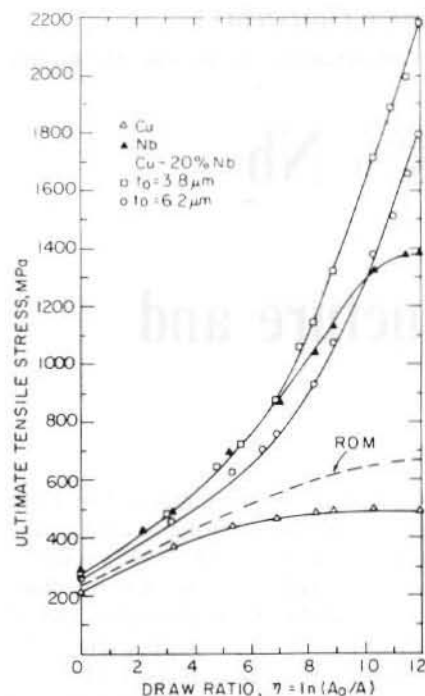
Fig. 2. Experimentally detected ultimate tensile strengths of pure Cu, pure Nb and Cu-20 mass% Nb [12].

[13, 14] have suggested a physical model which accounts for the observed dislocation structures and for the crystallographic textures of both phases without employment of fitting parameters.

ii. From a technical and commercial point of view the combination of high strength and good electrical conductivity makes Cu–Nb based MMCs highly potential candidate materials for the production of mechanically stressed electrical devices such as application in long-pulse high-field resistive magnets [15, 16].

Whereas the microstructure of Cu-20 mass% Nb has been subject to various studies in the past, its rigorous correlation with the mechanical behavior as well as corresponding simulations which are based on entirely physical rather than on semi-empirical models have not yet been submitted. Furthermore, recent experimental findings such as the occurrence of structurally less ordered, i.e. glassy areas in the Nb filaments [17] as well as the impact of texture on strength have not yet been discussed at all.

## 2 Fabrication of Cu–Nb in situ Composites

The Cu–Nb system reveals negligible mutual solubility in the solid state [1, 2] (Fig. 3). The strong difference of the melting points ($T_{Cu} = 1356$ K, $T_{Nb} = 2740$ K) indicates that in the as-cast ingots a dendritic grain structure is obtained. The morphology of the grains is dominantly predetermined by the melting, casting and cooling conditions. By imposing large degrees of plastic deformation the initial dendrites form into elongated filaments [3 to 13]. Cu–Nb MMCs reveal a considerable dependence of the extent and behavior of their coexisting phases on compositional deviations. Interstitial impurities like O, N, S and C are of major importance for deviations from the equilibrium phase diagram [2]. The nearly horizontal shape of the liquidus curve suggests a flat course of the Gibbs free energy curve over a wide compositional regime [1]. Accordingly, one has to take

into account the occurrence of a miscibility gap when interstitial impurities are present. Among these, O is supposed to have the strongest impact [2].

For the production of cast Cu-20 mass% Nb ingots the medium frequency induction melting technique was applied [18 to 20]. For this purpose an induction frequency of 10 kHz, a maximum coil voltage of 250 V and a maximum generator power of 30 kW were used [18, 19]. The complete aggregate was capsuled to allow for application of vacuum or inert gas atmosphere. Up to about 2125 K the temperature was measured pyrometrically. For cleaning the furnace chamber prior to melting of the composite, an initial vacuum of 10^{-4} mbar was produced. Subsequently, the furnace was filled with argon and evacuated again. The initial Cu melt was then prepared under a vacuum of 1.3×10^{-3} mbar. During melting of the Cu the Nb remained solid. After reaching the melting point of Cu the furnace chamber was filled with argon up to a pressure of 0.8 bar. According to the Cu–Nb equilibrium phase diagram [1] a melting temperature of at least 2000 K is recommended for Cu-20 mass% Nb (Fig. 3a). However, with increasing impurity content a melting temperature of at least 2075 K to 2125 K appears necessary (Fig. 3b) [2]. Since the exact content of interstitial foreign atoms in the Nb was not known, the melting temperature was raised up to about 2125 K to
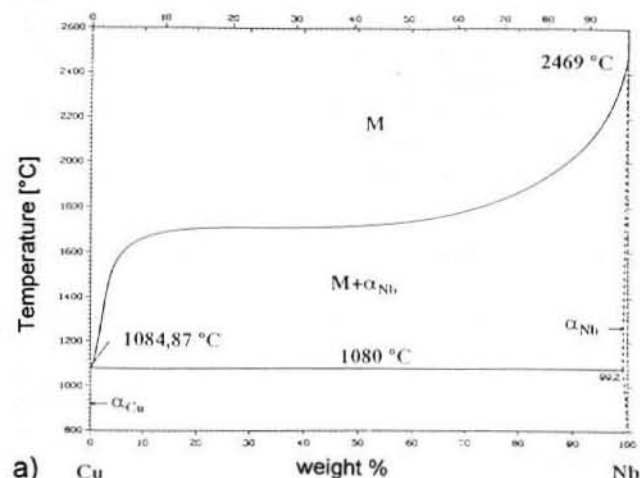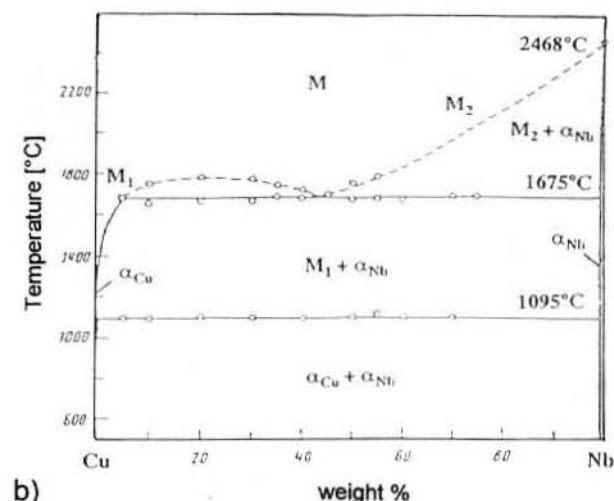
Fig. 3a and b. Phase diagrams of Cu and Nb. a) Pure constituents [1], b) impure constituents [2].
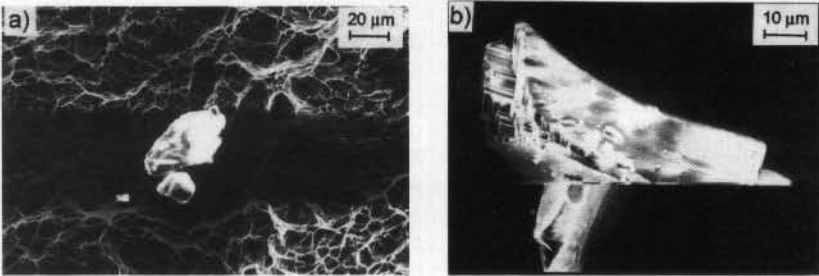
Fig. 4a and b. Small Nb crystals found in the cross-sections of broken wires.

assure the entire dissolution of the Nb. Insufficient melting temperatures allowed for the survival of small Nb crystals which were subsequently found within the fracture surfaces of broken wires (Fig. 4). It can be assumed that they are the main source for material failure during wire drawing. The mixing of the melt was achieved due to convection currents produced by the electromagnetic stirring effect. Subsequently, ingots of 18 mm diameter were cast under an argon atmosphere at a pressure of 0.8 bar. For the cast a crucible and a mould of high purity graphite were used. Since Cu based alloys are commonly not very suitable for intricate shape forming, the mould had to be preheated to nearly 900 K in order to improve flow characteristics. Since Cu and Nb reveal almost equal densities ($\varrho_{Cu} = 8890$ kg/m^3, $\varrho_{Nb} = 8580$ kg/m^3) gravitational segregation does thus not occur.

From the as-cast ingots wire drawn and cold rolled specimens were manufactured. The wires were processed by rotary swaging and subsequent drawing through hard metal drawing bench dies without intermediate annealing. The final diameter of the wires was 0.12 mm which represents a logarithmic deformation or true strain of $\eta = 10$ ($\varepsilon = 99.995\%$). In the composite wires, minimum fiber spacing of about 50 nm were found after $\eta = 10$. Additionally, as-cast Cu-20 mass% Nb samples were cold rolled to a final thickness of 0.06 mm, which corresponds to a true strain of $\eta = 5.2$ ($\varepsilon = 99.4\%$). In case that Cu based composites are used for the production of electrical coils the stability of the microstructure against heating had to be investigated. For this purpose various heat treatments were carried out, some of them directly during observation in the TEM.

3 Crystallographic Textures
3.1 Experimental

For texture investigations, wire drawn and cold rolled specimens were prepared from various deformation degrees [18, 20 to 23]. From the incomplete X-ray pole figures [24] {111}, {200}, {220}, {311} (Cu) and {110}, {200}, {112} (Nb) the orientation distribution functions (ODFs) were

computed using the Fourier type series expansion method ($l_{max} = 22$) [25]. The ODFs were approximated by Gaussian model functions [26] for error corrections which stem from the absence of the odd-order Fourier coefficients. For the examination of the microtexture specimens were prepared for scanning electron microscopy (SEM). By use of the electron back scattering diffraction (EBSD) technique, single grain orientation measurements were carried out [22, 23, 27]. The results are presented by use of inverse pole figures and ODFs.

3.2 Results

As is evident from Fig. 5 (electron diffraction) and Fig. 6 (X-ray diffraction), quantitative micro- and macrotexture investigations both supply consistently reliable texture data. The undeformed material elucidates a random orientation distribution of the Cu phase (Figs. 5a, 6a). With increasing deformation ($\varepsilon = 98.7\%$, $\eta = 4.3$) a Cu texture is generated which is described by a fiber axis between $\langle 111 \rangle$ and $\langle 100 \rangle$ (Figs. 5b, 6b). After heavy wire deformation ($\varepsilon = 99.98\%$, $\eta = 8.6$) two texture fibers are developed. The first one is characterized by a $\langle 111 \rangle$ and the second one by a $\langle 100 \rangle$ direction parallel to the drawing axis (Fig. 5c). The orientation density of the $\langle 111 \rangle$ fiber exceeds that of the $\langle 100 \rangle$ fiber. Both the results achieved by electron diffraction (Fig. 5) and by X-ray diffraction (Fig. 6) substantiate that the intensity of the $\langle 111 \rangle$ fiber increases, whilst that of the $\langle 100 \rangle$ fiber remains fairly stable on a low level during
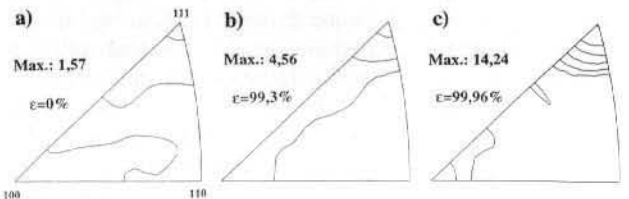

Fig. 6a to c. Texture of the Cu phase in the wire drawn MMC, X-ray diffraction. a) Undeformed material. b) Increasing deformation ($\varepsilon = 98.7\%$, $\eta = 4.3$). c) Heavy deformation ($\varepsilon = 99.98\%$, $\eta = 8.6$).
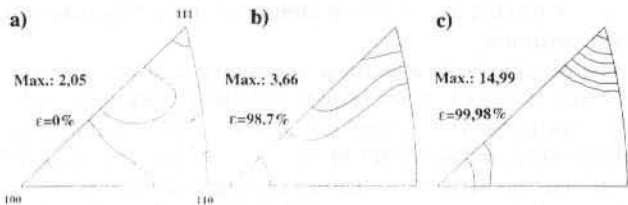

Fig. 5a to c. Texture of the Cu phase in the wire drawn MMC, electron diffraction. a) Undeformed material. b) Increasing deformation ($\varepsilon = 98.7\%$, $\eta = 4.3$). c) Heavy deformation ($\varepsilon = 99.98\%$, $\eta = 8.6$).
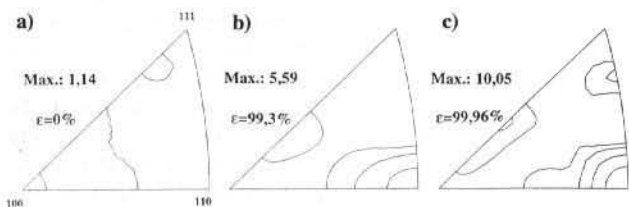

Fig. 7a to c. Texture of Nb phase in the wire drawn MMC, X-ray diffraction. a) Undeformed material. b) Increasing deformation ($\varepsilon = 98.7\%$, $\eta = 4.3$). c) Heavy deformation ($\varepsilon = 99.98\%$, $\eta = 8.6$).
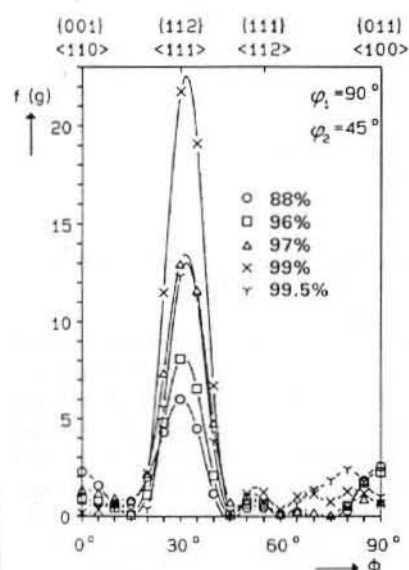
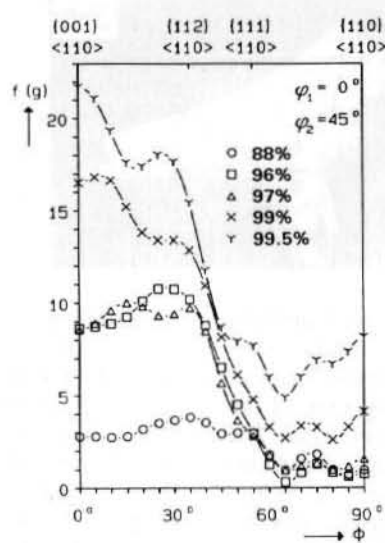Fig. 8. Texture of the Cu phase in the cold rolled MMC, X-ray diffraction.

Fig. 9. Texture of the Nb phase in the cold rolled MMC, X-ray diffraction.

In case of cold rolling, the texture deviates only in case of Nb from that observed for pure samples. Especially the formation of a strong $\{111\}\langle110\rangle$ orientation already after weak degrees of rolling deformation suggests local relaxation of the shear constraint in transverse direction. This behavior is attributed to the fact that the Cu phase has a low yield strength and allows hence for transverse shear of the Nb filaments [18].

4 Microstructure

4.1 Microscopy and Specimen Preparation

heavy deformation. In the Nb phase of the wire drawn samples a $\langle110\rangle$ texture fiber parallel to the drawing direction is generated after strong deformation ($\varepsilon > 98\,\%$, $\eta = 4$). For lower deformations ($\varepsilon < 98\,\%$, $\eta = 4$) the Nb texture remains very weak (Fig. 7a to c).

During rolling, in the Cu phase of the MMC a typical deformation texture is developed, which includes $\{112\}\langle111\rangle$ (Fig. 8), $\{123\}\langle634\rangle$ and $\{110\}\langle112\rangle$. In the Nb ribbons a strong α-fiber including $\{001\}\langle110\rangle$, $\{112\}\langle110\rangle$ and $\{111\}\langle110\rangle$ is formed already after low degrees of deformation (Fig. 9).

3.3 Discussion

For low and intermediate degrees of deformation the texture evolution of wire drawn and rolled Cu and Nb in the MMC corresponds to the results observed for single-phase material [18, 20 to 23]. Since texture analysis sensitively reflects crystallographic mechanisms, for low and intermediate strains the current results do hence not substantiate a striking difference between the deformation mechanisms which occur in single-phase and in MMC samples. An important feature of the results obtained for the wire drawing is, however, the retardation of the texture evolution. Whereas the texture in single-phase Cu and Nb wires becomes already pronounced during weak deformation, the wire texture observed in the MMC is developed only after heavy deformation. This retardation of texture evolution is attributed to the deformation state occurring during wire drawing. As will be discussed subsequently, after $\varepsilon = 80\,\%$ ($\eta = 1.6$) only very weak deformation of the Nb phase has taken place. In this strain regime most of the MMC deformation has been accomplished by the Cu matrix. In this first stage of drawing (up to $\varepsilon = 80\,\%$, $\eta = 1.6$) merely the dendrite arms which initially had a perpendicular orientation with respect to the dendrite axis, as well as the dendrite axis of the Nb phase itself, were rotated parallel to the drawing axis without essentially decreasing their diameters.

Whereas the substructure of the Cu phase has been subject to various studies [7, 9, 27, 28], the microstructure of the Nb filaments has not yet been studied on a similar level [30]. In the current study the morphology, topology as well as the average spacing have been quantitatively examined for both phases by use of scanning (SEM) and transmission electron microscopy (TEM). However, special attention was drawn to the studies of the substructure of the Nb filaments. In case of wire drawn MMC samples the preparation of isolated Nb filaments is highly intricate. Hence, in order to receive quantitative data, the investigation of the Nb substructure was essentially carried out on rolled rather than on wire drawn samples.

To avoid mechanical loading and heating of the specimens a new TEM foil preparation technique was developed which especially allowed for a thorough examination of the filaments. For providing flat sections, rolled samples were first cleaned in alcohol using ultrasonic vibrations. Subsequently, a thin Cu layer of some microns was removed by etching with a solution of 50 ml H_3PO_4 and 50 ml H_2O ($T = 268$ K, $U = 20$ V). This solution exclusively affects the Cu matrix, whereas HNO_3 etches both, Cu and Nb. After etching the specimen was cleaned again and then etched in a solution of 50 ml alcohol, 50 ml HF and 20 to 30 ml HNO_3 ($T = 300$ K, $U = 0$ V). By use of this solution the Nb filaments which outlasted the first etching were dissoluted. This successive procedure was repeated until perforation was nearly achieved. The last etching was then carried out by carefully dissolving the residual Cu close to the hole. As a result the Nb filaments were carefully extracted and isolated from the Cu matrix. To achieve equal thinning of both phases some samples were treated conventionally, viz. by use of mechanical thinning, dimpling and subsequent ion beam treatment.

The samples were examined employing a JEOL 2000FX operated at 200 kV using bright-field (BF), dark-field (DF) and selected area electron diffraction (SAD) techniques. Additionally, a JSM 6100 SEM was applied. For directly observing the structural regularity, high resolution transmission electron microscopy (HRTEM) was applied. For this purpose a JEOL 2000EX operated at 200 kV was used. The chemical analysis was locally determined by use of energy-dispersive X-ray spectrometry (EDX).
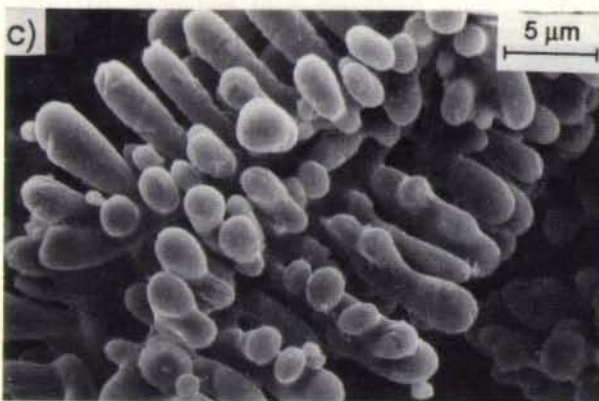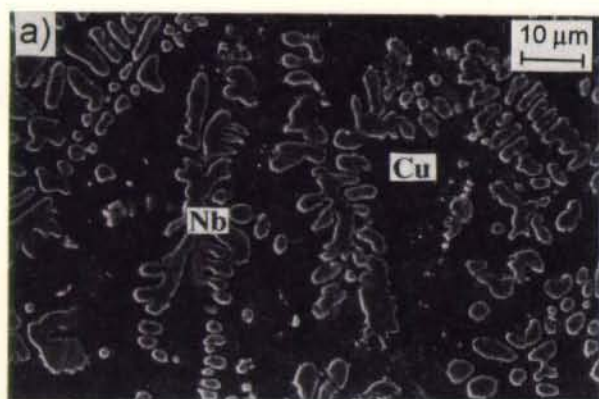
Fig. 10a to c. SEM micrographs of as-cast Cu-20 mass% Nb, a) Cross-section, primary Nb dendrites in Cu matrix. b) Isolated Nb dendrites, Cu matrix dissolved. c) Isolated Nb dendrites, Cu matrix dissolved. Dendrites up to third generation can be recognized.

Fig. 11a to c. SEM micrographs of Nb filaments, isolated by dissolving the Cu matrix at different degrees of wire deformation, a) $\varepsilon = 88.9\%$, b) $\varepsilon = 94.8\%$, c) $\varepsilon = 99.995\%$.

4.2 Microstructure of the Wire Drawn Samples
4.2.1 Results

Figure 10a shows the microstructure of the as-cast Cu-20 mass% Nb composite. The primary Nb dendrites (light) are embedded in the Cu matrix (dark). After selectively dissolving the Cu matrix by use of HNO_3, quantitative metallography was carried out on isolated dendrites (Fig. 10b). From Fig. 10c it is evident that the dendrites branch out up to the third generation. Whereas the orientations of the primary Nb dendrites are randomly distributed in the as-cast samples, the dendritic arms are commonly aligned parallel to the crystallographic $\langle 100 \rangle$ directions. The mean diameter of the secondary dendrites amounted to
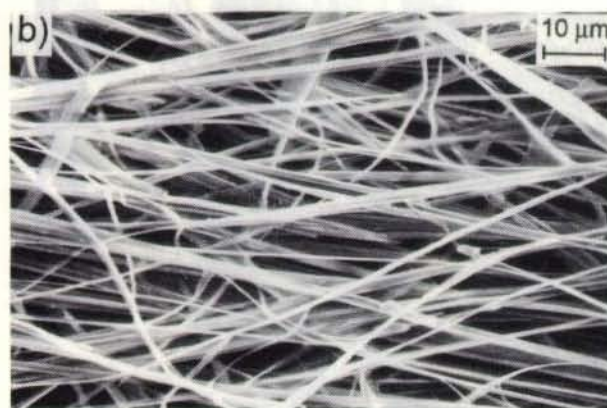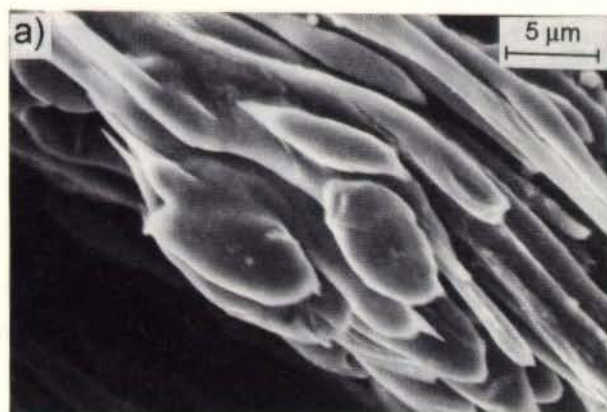
$d_0 = 2.2 \pm 0.4$ μm. The initial dendrite diameter as well as the degree of subsequent cold deformation determine the mechanical properties (Hall-Petch type hardening contribution of internal phase boundaries) and the electromagnetic properties (inelastic scattering of conduction electrons at internal phase boundaries) of the latter wire or sheet.

The evolution of the morphology of the Nb dendrites into elongated fibers is evident from Fig. 11a to c. After small amounts of deformation (Fig. 11a) ($\varepsilon = 88.9\%$, $\eta = 2.2$) the Nb morphology appeared quite inhomogeneous. Whereas some dendrite arms revealed considerable elongation, others appeared almost undeformed (Fig. 11a). Higher amounts of deformation ($\varepsilon = 94.8\%$, $\eta = 3$) resulted
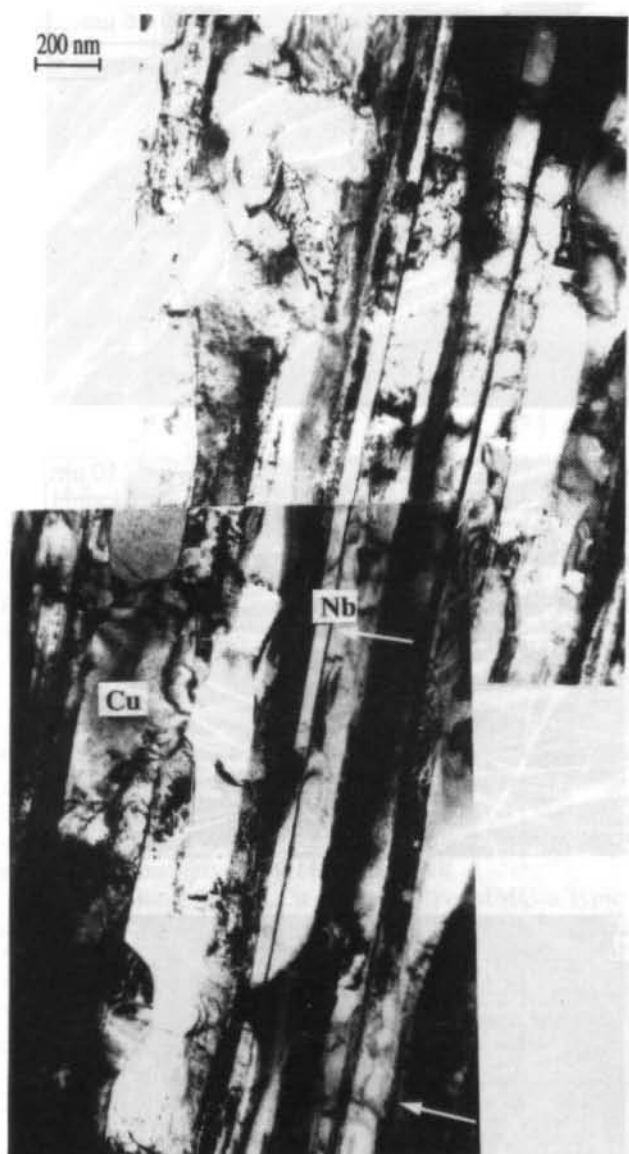
Fig. 12. TEM micrograph of wire drawn Cu-20 mass% Nb. Some small Nb filaments are indicated by arrows.

in filaments of a more uniform shape (Fig. 11b). The ultimate deformation ($\varepsilon = 99.995$ %, $\eta = 10$) led to an average fiber diameter of about 130 nm and a filament thickness of 60 nm. The smallest filaments, however, revealed a thickness less than 50 nm (Fig. 11c). Some fibers consisted of a thick part with elongated thin tails (Fig. 11c). In the heavily deformed in situ MMC all filaments were aligned parallel to the wire axis [13, 16, 17]. The random orientation distribution of the dendrite axes, as shown in the micrographs of Fig. 11, is an artifact from the SEM sample preparation. In order to quantitatively examine also the minimum occurring filaments, TEM measurements were additionally employed (Fig. 12). Some of the smallest Nb filaments are indicated by arrows.

The evolution of the deformation of the Nb filaments, as calculated from the metallographic data, is given as a function of the wire deformation in Fig. 13. The curve basically shows a linear dependence, although not a one to one correspondence. According to Fig. 13, a wire deformation of $\eta = 10$ ($\varepsilon = 99.995$ %) corresponds to a Nb filament

deformation of $\eta = 5.75$ ($\varepsilon = 99.68$ %). The actual deformation of the Nb phase was thus generally lower than expected for a homogeneous deformation of the wire. In the transverse section the folded morphology of the Nb filaments, which is referred to as curling, can be observed after a deformation of $\eta = 7.6$ ($\varepsilon = 99.95$ %) (Fig. 14). The wire hardness (200 g Vickers) is depicted as a function of deformation in Fig. 15. In the as-cast condition a value of about HV80 was measured. The hardness attained a
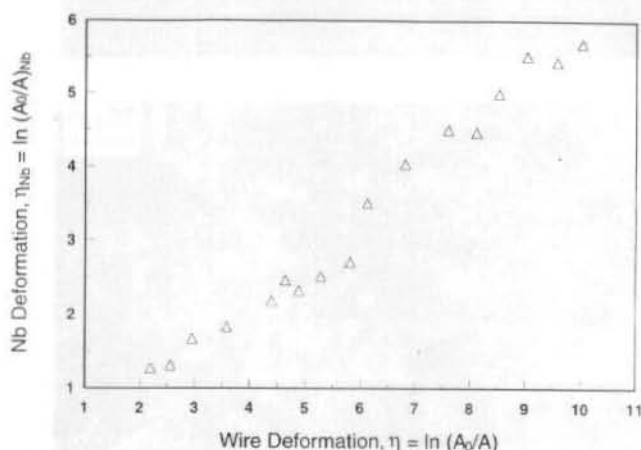

Fig. 13. Deformation of the Nb filaments as a function of the wire deformation.
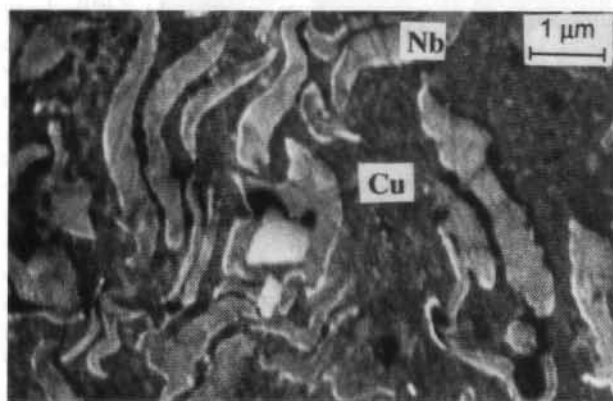

Fig. 14. Cross-section of a Cu-20 mass% Nb wire, $\eta = 7.6$ ($\varepsilon = 99.95$), the curling of the filaments becomes apparent.
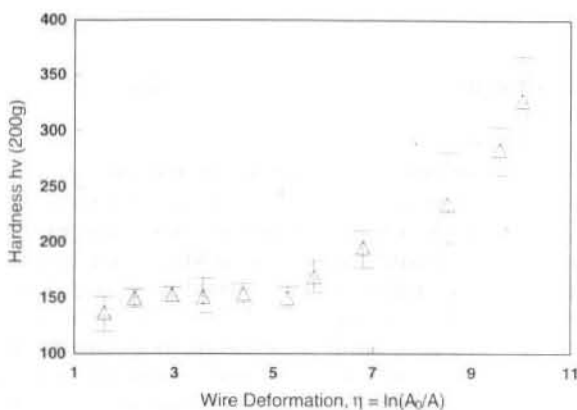

Fig. 15. Change of microhardness (Vickers, 200 g) of Cu-20 mass% Nb with increasing wire deformation.
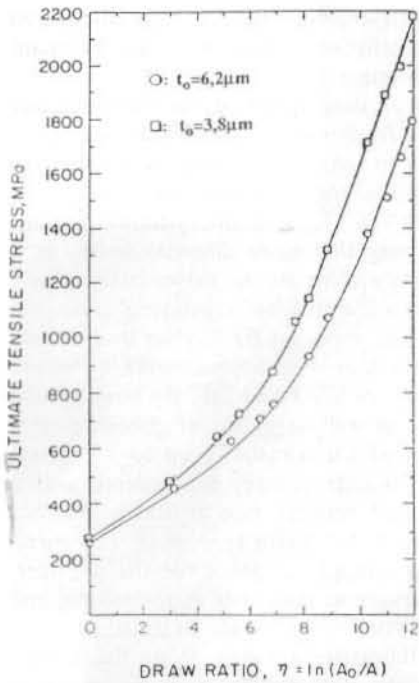
Fig. 16. Ultimate tensile strength versus draw ratio, two different initial dendrite diameters [29].

plateau value of HV150 within the range $2 \leq \eta \leq 6$. At large deformation ($\eta > 6$) a strong increase of the hardness was observed, extending to a maximum value of HV325 at $\eta = 10$ ($\varepsilon = 99.995$ %).

4.2.2 Discussion

The average diameter of the secondary dendrites was about 2 µm. Compared with other production methods this value is quite small [5 to 10] and thus ensures a high tensile strength after heavy deformation (Fig. 16). The high cooling rate did not only lead to a small dendrite diameter but also to a higher density of dendrites of second and third generation.

The observed inhomogeneous Nb morphology up to a deformation degree of $\eta \approx 2$ ($\varepsilon = 87$ %) (Fig. 11a) substantiates that very heavy deformation is necessary to produce a homogeneous size distribution of the Nb filaments within the MMC (Fig. 11b, c). This is explained by several reasons. Firstly, the strain distribution during wire drawing is inhomogeneous across the wire diameter resulting in an inhomogeneous dendrite morphology. Secondly, small degrees of deformation cause the initially randomly oriented dendrites [18, 22, 23] to rotate towards an orientation parallel to the wire axis as indicated by the lower deformation of the Nb dendrites compared with the Cu matrix (Fig. 13). This is also confirmed by the hardness plateau observed for $\eta < 6$ ($\varepsilon = 99.8$ %) (Fig. 15). After this alignment ($\eta \approx 6$) a massive cross-sectional area reduction of the dendrites took place. These observations correspond to the finding that with regard to strength considerable deviations from the predictions of the linear rule of mixtures (ROM) were observed for high ($\eta > 6$) but not for low degrees of deformation. This is apparently the reason that for $\eta \approx 2$ ($\varepsilon = 87$ %) (Fig. 11a) a mixture of highly deformed dendrites and almost undeformed ones were found next to each other. Moreover, the deformation is strongly influenced by the incompatibility of the deformation of the fcc Cu and the bcc Nb phase. Since the distribution of the Nb is inhomogeneous, the more

ductile Cu phase has to undergo a higher deformation locally. This again modifies the local stress distribution within the wire, i.e. neither the actual Cu deformation nor the actual Nb deformation equals the true wire deformation.

After heavy deformation of the MMC all Nb filaments are aligned parallel to the wire axis. As noted before, the random orientation of the fibers in Fig. 11 is an artifact introduced during specimen preparation. The strong bending of the filaments occurring subsequent to dissolving the Cu matrix indicates strong residual stresses, i.e. a high content of geometrically necessary dislocations. Another striking feature of the Nb filaments is their flat and curled morphology when observed in the cross-section of the wire (Fig. 14). While the wire deformation imposes a strain state with rotation symmetry about the drawing direction, the resulting shape of the Nb filaments does not reveal this symmetry. This had to be attributed to the microscopic strain distribution and can be explained by the orientation distribution of the Nb filaments. As is evident from texture experiments and Taylor simulations, the bcc Nb phase develops a $\langle 110 \rangle$ fiber texture during wire deformation ($\eta > 4$) [20 to 23]. According to Hosford [31], this texture allows for only two of the four $\langle 111 \rangle$ bcc slip directions to contribute to plastic deformation parallel to the wire axis. However, the activation of only 2 symmetrical slip systems causes a local plane strain deformation which leads, under the externally imposed axisymmetric flow, to a bent shape of the Nb phase, which is referred to as curling. This phenomenon only occurs in composites which consist of a bcc and a fcc phase. In fcc metals, where usually a $\langle 111 \rangle$ texture is generated during wire drawing, no planar slip is enforced, i.e. accordingly no curling is observed in
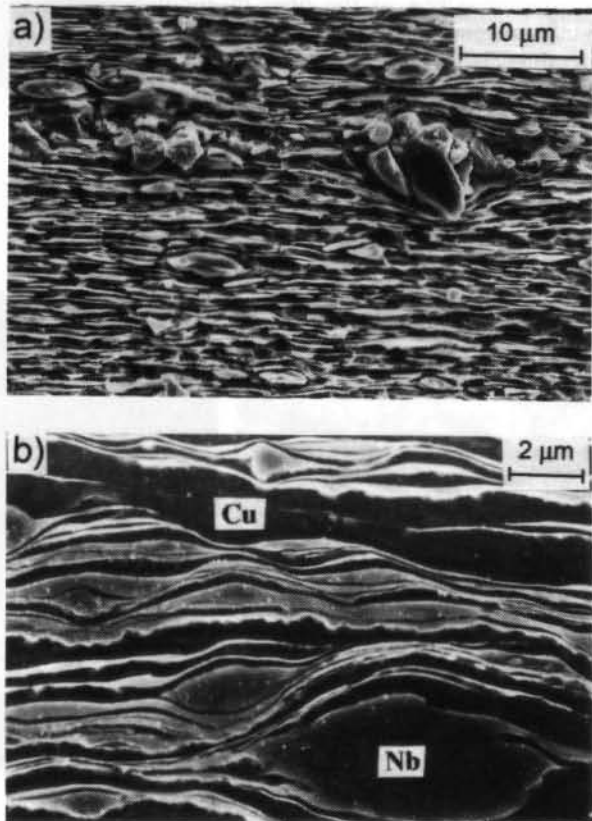

Fig. 17a and b. Transverse section of rolled Cu-20 mass% Nb, a) $\varepsilon = 95$ %, b) $\varepsilon = 99.4$ %.
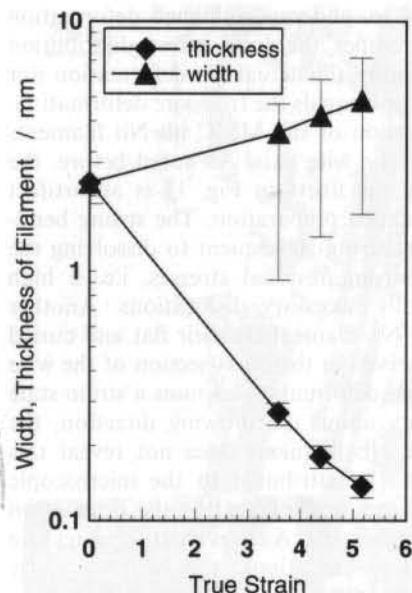
Fig. 18. Development of the filament width and thickness as a function of rolling deformation.

composites consisting of two fcc phases. The most significant consequence of the Nb curling is the strong increase of the total Cu–Nb phase boundary area.

4.3 Microstructure of the Cold Rolled Samples
4.3.1 Results

The evolution of the Nb dendrites into elongated filaments during cold rolling is shown in Fig. 17. Even after heavy deformation ($\varepsilon = 99.4\%$) the fiber morphology appeared quite inhomogeneous. Whereas some dendrites revealed considerable flattening, others appeared much less deformed (Fig. 18). In the filaments of the three highest deformation degrees, intricate dislocation arrangements were observed, consisting of elongated dislocation cells (Fig. 19a) and densely arranged tangles with maximum dislocation densities of up to 10^{16} m^{-2} (Fig. 19b). Even though some areas containing only few elongated disloca-

tions with densities not exceeding 10^{12} m^{-2} were discovered (Fig. 19c), dislocation cells and tangles were the dominant elements of the substructure.

However, the most exciting result of the present study was the discovery of structurally less ordered, i.e. amorphous or glassy areas in many Nb filaments which were extracted from samples cold rolled to $\varepsilon = 97.2\%$, $\varepsilon = 98.8\%$ and $\varepsilon = 99.4\%$. These non-crystalline regions frequently expanded over the entire filament width. It is essential to painstakingly differentiate between the glassy state and simply dislocation free but crystalline areas, the occurrence of which was reported by Trybus and Spitzig [9]. For this purpose the loss of structural regularity was in all cases checked by use of SAD and DF. By employment of EDX in the glassy as well as in the neighboring crystalline areas an enhanced Cu content of up to 3.5 mass% was detected. In Fig. 20 a structurally less ordered area is revealed. It is positioned between two crystalline regions and extends over the filament width ($\varepsilon = 99.4$). The corresponding SAD patterns supply evidence for the considerable degradation of structural regularity in the middle and the preservation of crystalline structure in adjacent areas (Fig. 20). Whereas the pattern taken from the middle region clearly reveals the diffuse diffraction circles which are typically generated by less ordered materials, both adjacent regions reveal not only crystalline diffraction patterns but additionally similar orientations. An important feature of the micrographs taken from the glassy areas is the absence of the thickness contrast lines. If the filaments under investigation were very thin, the state of structural order in the glassy areas was additionally checked by employing HRTEM. As is evident from the micrograph shown in Fig. 21, the strict structural regularity of the atoms is partially destroyed and partially maintained. In numerous areas the initial crystal planes are no longer discernible but appear wavy and disintegrated. These results substantiate that the atomic structure observed within those regions in which diffuse diffraction circles were produced by SAD, was not entirely amorphous but glassy or even nano-crystalline. If conventional TEM preparation techniques were used, i.e. mechanical thinning, dimpling and ion beam bombardment (Fig. 12), no glassy areas were observed.
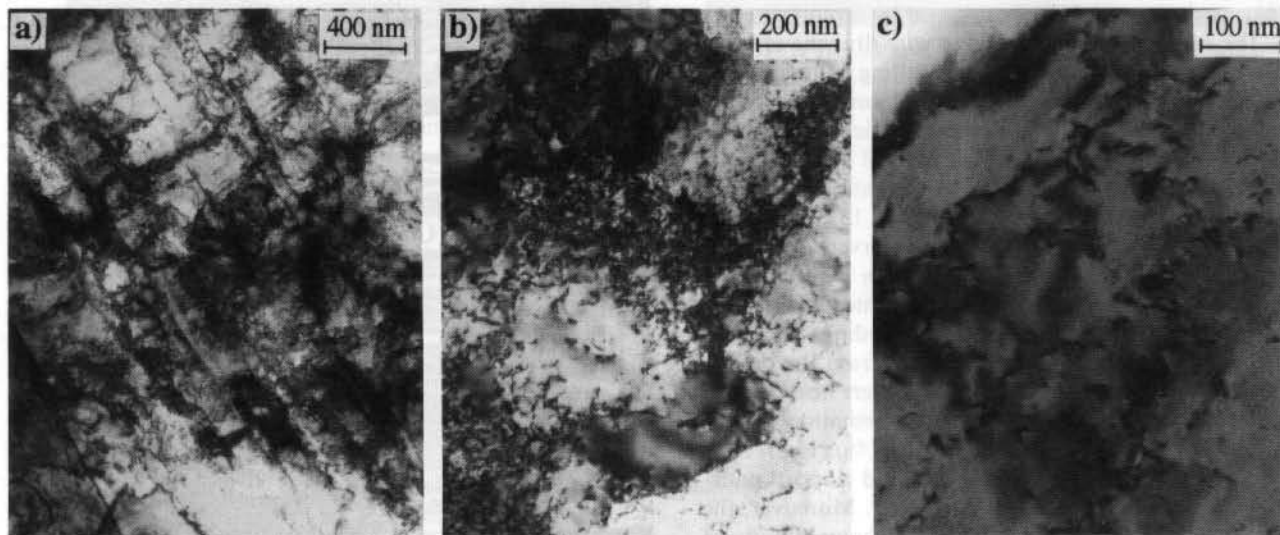

Fig. 19a to c. Dislocation arrangements in the Nb filaments, extracted from rolled samples ($\varepsilon = 99.4\%$). a) Cells. b) Tangles. c) Single dislocations.
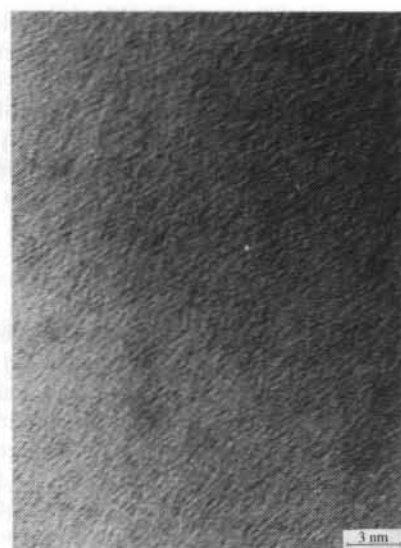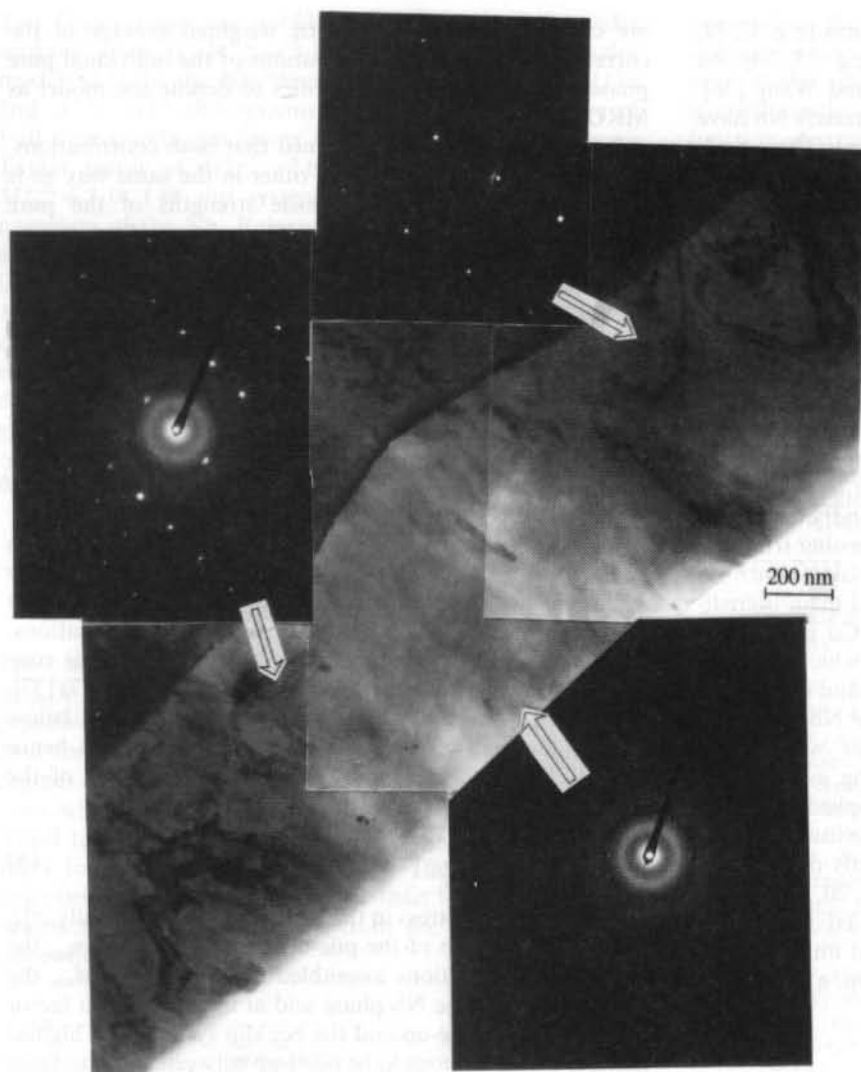
200 nm

Fig. 21. HTEM micrograph taken from a structurally less ordered area in a Nb filament, extracted from a rolled sample.

Fig. 20. Structurally less ordered area in a Nb filament, extracted from a rolled sample ($\varepsilon = 99.4\%$). SAD diffraction patterns indicate glassy or nanocrystalline area in the filament.

4.3.2 Discussion

After low and even after heavy rolling deformation the thickness distribution of the filaments appears very inhomogeneous in the rolled MMC. As already expounded for wire drawn specimens this is essentially attributed to the inhomogeneous distribution of stress. After the highest deformation investigated ($\varepsilon = 99.4\%$) an average filament thickness of 104 nm and minimum values of less than 50 nm were found (Fig. 18). The average filament width after $\varepsilon = 99.4\%$ was about 4000 nm (Fig. 18).

The appearance of structurally less ordered areas in the Nb fibers [32] is the most interesting discovery. In various studies on wire drawn [7, 27] and rolled [9] Cu-20 mass% Nb the microstructural evolution of the Nb filaments was investigated by use of TEM. Albeit the dislocation arrangements and densities found there [7, 27, 9] were very similar to those observed in the present study, the occurrence of glassy areas was not mentioned in former publications. This disagreement is essentially attributed to the different TEM foil preparation method [32]. In the present study the essential step was the introduction of a new technique which allowed for a low preparation temperature less than 300 K. At this temperature regime premature crystallization of the glassy areas can be excluded. In all previous TEM

studies on deformed Nb filaments, however, [e.g. 7, 9], mechanical grinding, dimpling and subsequent ion beam bombardment was employed. This conventional procedure gives rise to an enhanced sample temperature prior to observation. It is hence likely that in previous studies crystallization of initially glassy areas had taken place during sample preparation. This is also underlined by the fact that in the present study no glassy areas were observed when the conventional foil preparation method was employed. Furthermore, in previous works longitudinal and transverse sections, but no flat sections were investigated [7, 9, 27]. In this investigation it was exclusively made use of the latter type of sections, the examination of which allows for statistically more reliable observations, since numerous structurally less ordered areas extended over the entire filament width.

In the glassy as well as in the adjacent crystalline areas an enhanced Cu content was detected. In addition, the graphite crucible used to prepare the melt, is known to promote an increased content of N, C and S [19, 20]. This fact was confirmed by the high electrical resistivity of the as-cast ingot [11]. The enhanced impurity content, however, is a necessary precondition for the formation of metallic glass, since very pure metals were never transformed into the amorphous state. Metallic glasses consisting either of 4d-transition metals (e.g. Nb) and 4s-metals (e.g. Cu), or a

transition metal (e.g. Nb) and metalloid atoms (e.g. C, N, S, B, Si), have frequently been observed [e.g. 33, 34]. As reported by Wang et al. [35] and Iwasaki and Wang [36], amorphous alloys containing more than 80 mass% Nb have been produced by employing rapid quenching. These findings underline the present observation, viz. that Nb potentially reveals the tendency to undergo phase transformation into a structurally less ordered state.

5 Simulation of the Yield Strength

In former models [8, 10] the increase of strength is described in terms of various parameters fitted to experimental flow curves. In the present work a physical model is introduced. The new approach is a modified linear rule of mixtures (MROM). It regards the yield strength of the composite as the sum of the volumetric weighted average of the experimentally observed yield strengths of the individual pure phases and a Hall-Petch type contribution arising from the impact of the Cu–Nb phase boundaries. The latter contribution is analytically described in terms of two main ingredients. Firstly, by dislocation pile-ups in the Cu matrix and secondly, by the approach of Sevillano [37] which incorporates the activation of dislocation movement and multiplication in lamellar two-phase aggregates in the Nb filaments. The current model accounts essentially for wire drawn specimens. However, most of the underlying assumptions suggested in the following also can be applied to rolled samples. The dislocation arrangements, the textures and the distribution of the filament geometry presently observed as well as those reported by other authors [e.g. 20, 23, 28, 29] are considered. The TEM data [e.g. 28, 29] suggest an evolution of the Nb filament thickness t and interdendritic spacing λ as a function of the true wire strain, η, according to:

$$t = t^0 \cdot \exp(-A_{Nb} \cdot \eta_{MMC})$$

and

$$\lambda = \lambda^0 \cdot \exp(-A_{Cu} \cdot \eta_{MMC}) \qquad (1)$$

with starting values $t^0 = 1.2\ \mu m$ and $\lambda^0 = 6\ \mu m$ [29]. Accounting for the different deformation of both phases in the composite, the relations A_{Cu} and A_{Nb} are introduced:

$$A_{Cu} = \frac{\eta_{Cu}}{\eta_{MMC}}; \quad A_{Nb} = \frac{\eta_{Nb}}{\eta_{MMC}}; \quad \eta = \ln \frac{A^0}{A} \qquad (2)$$

where A^0 and A are the initial and the present cross-section, η_{MMC} the true strain of the bulk sample, η_{Nb} the strain of Nb and η_{Cu} that of the Cu phase. In the current model the deviation, $\Delta\sigma$, between the predictions of the linear rule of mixtures (ROM), σ_{ROM}, and the strength observed, $\sigma_{P0,2}$, is attributed to the presence of the filaments.

$$\sigma_{P0,2} = \sigma_{ROM} + \Delta\sigma \qquad (3)$$

Following the ROM the yield strength can be written as

$$\sigma_{ROM} = \sigma_{ROM}^{Cu} \cdot V_{Cu} + \sigma_{ROM}^{Nb} \cdot V_{Nb} \qquad (4)$$

where σ_{ROM}^{Cu} is the yield strength for pure Cu and σ_{ROM}^{Nb} that for pure Nb. V_{Cu} and V_{Nb} are the volume fractions of Cu and Nb, respectively. For $\Delta\sigma$ the same approach applies:

$$\Delta\sigma = \Delta\sigma^{Cu} \cdot V_{Cu} + \Delta\sigma^{Nb} \cdot V_{Nb} \qquad (5)$$

where $\Delta\sigma^{Cu}$ and $\Delta\sigma^{Nb}$ are the additional strength contributions, attributed to the impact of the filaments. From Eqs. (4) and (5) it is evident that both parts, σ_{ROM} and $\Delta\sigma$,

are calculated as the volumetric weighted average of the corresponding strength contributions of the individual pure phases. Such an approach justifies to denote the model as MROM.

In the following it was assumed that both contributions, $\Delta\sigma^{Cu}$ and $\Delta\sigma^{Nb}$, relate to each other in the same way as is observed for the ultimate tensile strengths of the pure constituents, σ_{ROM}^{Cu} and σ_{ROM}^{Nb}. The relation R was as a function of strain computed from experimental data.

$$\frac{\sigma_{ROM}^{Nb}}{\sigma_{ROM}^{Cu}} = \frac{\Delta\sigma^{Nb}}{\Delta\sigma^{Cu}} \equiv R \qquad (6)$$

The externally imposed stress which is carried by the Nb as well as the dislocation pile-ups in the Cu phase in front of the phase boundaries both contribute to the strength, τ_{VB}, which is required to initiate movement of dislocations in the Nb filaments [37]:

$$\tau_{VB} = \frac{A \cdot G \cdot b}{2\pi \cdot t} \cdot \ln\left(\frac{t}{b}\right); \quad A \equiv 1.2 \qquad (7)$$

where t is the filament thickness, G the shear modulus, b the Burgers vector and A a constant for mixed dislocations. If dislocation multiplication rather than movement is considered inside the filament, t is replaced by $t/2$ in Eq. (7) [37]. Since the thickness of the filaments is considerably below that of the matrix, the glide resistance in Nb will hence exceed that in the Cu phase. The stress at the tip of the pile-ups in the Cu phase can be written as

$$\tau_{tip}^{Cu} = \tau_{plp}^{Cu} \cdot n_{plp} = \frac{1}{m}\left(\tau_{VB} - \frac{\Delta\sigma^{Nb}}{M_{Nb}}\right) \qquad (8)$$

where $\Delta\sigma^{Nb}$ is the stress in the Nb as imposed externally, τ_{plp}^{Cu} the stress at the tip of the pile-up in the Cu phase, n_{plp} the number of dislocations assembled in the pile-up, M_{Nb} the Taylor factor of the Nb phase and m the orientation factor between the fcc pile-up and the bcc slip system. The highest number of dislocations to be piled-up between two interfaces results in [38]

$$n_{plp} = \frac{\tau_{plp}^{Cu} \cdot \lambda^+ \cdot (1 - v^{Cu})}{G_{Cu} \cdot b_{Cu}} \qquad (9)$$

where $\lambda^+ = \lambda/m_{Cu}$ and $t^+ = t/m_{Nb}$ are the distances corrected with respect to the orientation of the active slip system. Accordingly, m_{Cu} is the orientation factor of Cu and m_{Nb} that of Nb. From Eqs. (8) and (9) it follows

$$(\tau_{plp}^{Cu})^2 \cdot \frac{\lambda^+ \cdot (1 - v_{Cu})}{G_{Cu} \cdot b_{Cu}} = \frac{1}{m}\left(\tau_{VB} - \frac{\Delta\sigma^{Nb}}{M_{Nb}}\right) \qquad (10)$$

Incorporating $\Delta\sigma = M\tau$ as well as Eq. (6) this relation can be written as

$$\left(\frac{\Delta\sigma^{Cu}}{M_{Cu}}\right)^2 \cdot \frac{\lambda^+ \cdot (1 - v_{Cu})}{G_{Cu} \cdot b_{Cu}} = \frac{1}{m}\left(\tau_{VB} - R \cdot \frac{\Delta\sigma^{Cu}}{M_{Nb}}\right) \qquad (11)$$

resulting in

$$\Delta\sigma^{Cu} = -\frac{R \cdot M_{Cu}^2 \cdot G_{Ci} \cdot b_{Cu}}{2 \cdot \lambda^+ \cdot (1 - v_{Cu}) \cdot M_{Nb} \cdot m}$$
$$+ \sqrt{\left(\frac{R \cdot M_{Cu}^2 \cdot G_{Cu} \cdot b_{Cu}}{2 \cdot \lambda^+ \cdot (1 - v_{Cu}) \cdot M_{Nb} \cdot m}\right)^2 + \frac{\tau_{VB} \cdot M_{Cu}^2 \cdot G_{Ci} \cdot b_{Cu}}{\lambda^+ \cdot (1 - v_{Cu}) \cdot m}} \qquad (12)$$

The yield strength contributed by the presence of the filaments thus amounts to

$$\Delta\sigma = (V_{Cu} + V_{Nb} \cdot R) \cdot \Delta\sigma^{Cu} \qquad (13)$$

414

The Taylor factor for a $\langle 111 \rangle$ fiber texture of Cu under uniaxial load is $M_{Cu}^{fc12} = 3.16$ (Full Constraints Taylor model) [13]. In the Nb filaments $\{110\}\langle 111 \rangle$, $\{112\}\langle 111 \rangle$ and $\{123\}\langle 111 \rangle$ slip systems can be activated. In case of Full Constraints conditions the $\langle 110 \rangle$ oriented Nb has a Taylor factor of $M_{Nb}^{fc12} = 3.67$ ($\{110\}\langle 111 \rangle$ slip only) or $M_{Nb}^{fc48} = 3.18$ (48 slip systems). Due to the curling phenomenon of the Nb, Relaxed Constraints conditions were also considered. In case of $\{110\}\langle 111 \rangle$ slip the Taylor factor amounts to $M_{Nb}^{rc12} = 2.45$ and for 48 slip systems to $M_{Nb}^{rc48} = 2.15$. The orientation factors which were used to compute the resolved shear stresses were $m_{Cu} = 0.27$, $m_{Nb} = 0.4$ and $m = 0.98$. Using the lowest Taylor factors computed, the contribution of the fiber morphology to the yield strength of the composite then amounts to

$$\Delta\sigma = (0.8 + 0.2 \cdot R) \cdot \left(-\frac{4.25 \text{ MPa}}{M_{Nb}} \cdot R \right.$$
$$+ \left. \sqrt{\left(\frac{4.25 \text{ MPa}}{M_{Nb}} \cdot R\right)^2 + 5.9 \text{ MPa}^2 \cdot \left(9.25 - \frac{\eta}{2}\right)} \right) \cdot \exp\left(\frac{\eta}{2}\right)$$

$$(14)$$

The simulation (indicated as: ROM + MMC, i.e. $\sigma_{ROM} + \Delta\sigma$) reveals a very good correspondence to the experimental results (EXP) (Fig. 22). The experimental data for computing σ_{ROM} were taken from [12]. For high degrees of deformation the ultimate tensile strengths (UTS) from which the data of the ROM were computed correspond to the yield strengths (UTS $\approx R_{p0.2}$). This does not apply for low strains (UTS $> R_{p0.2}$). The model, however, describes the yield strength rather than the UTS. For low strains the data incorporated from the ROM are hence somewhat overestimated.
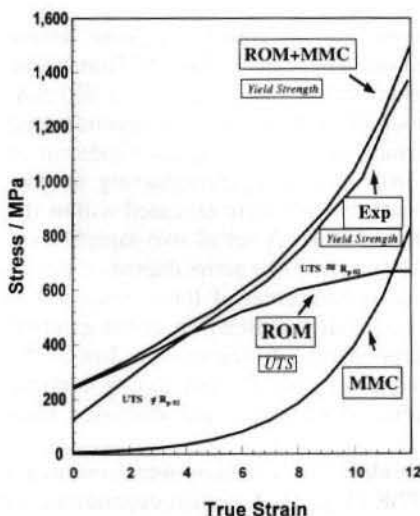

Fig. 22. Prediction of the yield strength of the MMC according to the new model. The simulation (indicated as: ROM + MMC, i.e. $\sigma_{ROM} + \Delta\sigma$) reveals a very good correspondence to experiment (EXP). The experimental data were taken from [12].

6 Conclusions

The fabrication, microstructure, texture and mechanical properties of heavily rolled and wire drawn Cu-20 wt.% Nb in situ composites have been studied. It was shown that the high strength of this MMC can be understood in terms of its microstructure. Especially the substructure of the Nb is essential for the strength of the MMC. In the Nb filaments dislocation cells, tangles and glassy areas were observed. A new model which describes the evolution of the yield strength on the basis of the microstructure and texture as a function of strain was introduced. The model yields a very good correspondence to experiment.

Literature

1. *Chakrabati, D. J.; Laughlin, D. E.:* Bull. Alloy Phase Diagrams 2 (1982) 936.
2. *Terekhov, G. I.; Aleksandrova, L. N.:* Izv. Akad. Nauk SSSR. Met. 4 (1984) 210.
3. *Frommeyer, G.:* Verbundwerkstoffe, DGM-Verlag (1981).
4. *Karasek, K. R.; Bevk, J.:* J. Appl. Phys. 52 (1981) 1370.
5. *Bevk, J.; Harbison, J. P.; Bell, J. L.:* J. Appl. Phys. 49 (1978) 6031.
6. *Bevk, J.; Karasek, K. R.:* in: D. Kuhlmann-Wilsdorf, W. C. Harrigan (eds.), New Developments and Applications in Composites, AIME, Warrendale, PA (1979) 101.
7. *Spitzig, W. A.; Pelton, A. R.; Laabs, F. C.:* Acta metall. 35 (1987) 2472.
8. *Spitzig, W. A.:* Acta metall. 39 (1991) 1085.
9. *Trybus, C.; Spitzig, W. A.:* Acta metall. 37 (1989) 1971.
10. *Funkenbusch, P. D.; Courtney, T. H.:* Acta metall. 33 (1985) 913.
11. *Raabe, D.; Heringhaus, F.:* phys. stat. sol. (a) 142 (1994) 473.
12. *Spitzig, W. A.; Krotz, P.:* Scripta metall. 21 (1987) 1143.
13. *Raabe, D.; Hangen, U.:* in: S. I. Andersen, J. B. Bilde-Sorensen, T. Lorentzen, O. B. Pedersen, N. J. Sorensen (eds.), Proc. 15th Risø Int. Symp. on Mat. Sc. on Num. Prediction of Def. Proc. and the Behav. of Real Mat., RISØ Nat. Lab, Roskilde, Denmark (1994) 487.
14. *Raabe, D.; Hangen, U.; Gottstein, G.:* Proc. Int. Workshop on "High-Strength, High-Conductivity Composite Mat.", Nat. High Magn. Field Lab., Tallahassee, Florida (1994).
15. *Embury, J. D.; Hill, M. A.; Spitzig, W. A.; Sakai, Y.:* MRS Bull. 8 (1993) 57.
16. *Schneider-Muntau, H.-J.:* IEEE Trans. Magn. 18 (1982) 32.
17. *Raabe, D.; Hangen, U.:* Mater. Lett., in press.
18. *Raabe, D.; Gottstein, G.:* J. de Phys. IV, col. C7, sup. J. de Phys. III 3 (1993) 1727.
19. *Heringhaus, F.; Raabe, D.; Kaul, L.; Gottstein, G.:* Zeitschrift Metall 6 (1993) 558.
20. *Heringhaus, F.; Raabe, D.; Gottstein, G.:* Metall 48 (1994) 287.
21. *Raabe, D.:* Dissertation, RWTH Aachen (1992).
22. *Raabe, D.; Ball, J.; Gottstein, G.:* Scripta metall. 27 (1992) 211.
23. *Heringhaus, F.; Hangen, U.; Raabe, D.; Gottstein, G.:* Mater. Sci. Forum 157–162 (1994) 709.
24. *Schulz, L. G.:* Appl. Phys. 20 (1949) 1030.
25. *Bunge, H. J.:* Z. Metallkd. 56 (1965) 872.
26. *Lücke, K.; Pospiech, J.; Virnich, K. H.; Jura, J.:* Acta metall. 29 (1981) 167.
27. *Engler, O.; Gottstein, G.:* Steel Research 63 (1992) 413.
28. *Pelton, A. R.; Laabs, F. C.; Spitzig, W. A.; Cheng, C. C.:* Ultramicroscopy 22 (1987) 251.
29. *Verhoeven, J. D.; Spitzig, W. A.; Schmidt, F. A.; Krotz, P. D.; Gibson, E. D.:* J. Mater. Sc. 24 (1989) 1015.
30. *Raabe, D.; Hangen, U.:* Acta metall., in press.
31. *Hosford, W. F. Jr.:* Trans. of TMS AIME 230 (1964) 12.
32. *Raabe, D.; Hangen, U.:* J. Mater. Res., in press.
33. *Luborsky, F. E.:* Amorphous Metallic Alloys, Butterworths, London (1983).
34. *Güntherodt, H. J.; Beck, H.:* Glassy Metals, Springer Verlag, Berlin, 1 (1981), 2 (1982).
35. *Wang, W. K.; Iwasaki, H.; Suryanarayana, G.; Masumoto, T.; Fukamichi, F.; Syono, Y.; Togo, T.:* in: T. Masumoto, K. Suzuki (eds.), Proc. 4th Int. Conf. on Rapidly Quenched Metals, Sendai, 1981, Jap. Inst. of Metals, Sendai RQ4 (1982) 663.
36. *Iwasaki, H.; Wang, W. K.:* Sci. Rep. of Res. Inst. of the Tohoku Univ. 29A (1981) 195.
37. *Sevillano, J. G.:* J. de Phys. III 6 (1990) 967.
38. *Chou, Y. T.:* phys. stat. sol. 17 (1966) 509.